

# Calcium Phosphate-Reinforced Metal-Organic Frameworks Regulate Adenosine-Mediated Immunosuppression

Ling Liang, Lei-Lei Yang, Wenjie Wang, Cailing Ji, Lei Zhang, Yiyi Jia, Yuxia Chen, Xueqiang Wang, Jie Tan,\* Zhi-Jun Sun,\* Quan Yuan,\* and Weihong Tan

Long-term accumulation of adenosine (Ado) in tumor tissues helps to establish the immunosuppressive tumor microenvironment and to promote tumor development. Regulation of Ado metabolism is particularly pivotal for blocking Ado-mediated immunosuppression. The activity of adenosine kinase (ADK) for catalyzing the phosphorylation of Ado plays an essential role in regulating Ado metabolism. Specifically, accumulated Ado in the tumor microenvironment occupies the active site of ADK, inhibiting the phosphorylation of Ado. Phosphate can protect ADK from inactivation and restore the activity of ADK. Herein, calcium phosphate-reinforced iron-based metal-organic frameworks (CaP@Fe-MOFs) are designed to reduce Ado accumulation and to inhibit Ado-mediated immunosuppressive response in the tumor microenvironment. CaP@Fe-MOFs are found to regulate the Ado metabolism by promoting ADK-mediated phosphorylation and relieving the hypoxic tumor microenvironment. Moreover, CaP@Fe-MOFs can enhance the antitumor immune response via Ado regulation, including the increase of T lymphocytes and dendritic cells and the decrease of regulatory T lymphocytes. Finally, CaP@Fe-MOFs are used for cancer treatment in mice, alleviating the Ado-mediated immunosuppressive response and achieving tumor suppression. This study may offer a general strategy for blocking the Ado-mediated immunosuppression in the tumor microenvironment and further for enhancing the immunotherapy efficacy *in vivo*.

## 1. Introduction


Adenosine (Ado) is an important signaling molecule that can regulate many physiological processes, such as hypoxia, ischemia, inflammation, or trauma.<sup>[1]</sup> In normal tissues, Ado has a protective effect against cells and tissues from the excessive inflammation and immune response-mediated damage.<sup>[2]</sup> However, in the tumor microenvironment, abnormal tumor metabolism leads to excess Ado that helps to establish the immunosuppressive tumor microenvironment.<sup>[3]</sup> A growing number of reports have pointed out that Ado inhibits the activation of immune response and plays a notable role in the evasion of antitumor immune response.<sup>[4]</sup> Ado can bind to the Ado receptors on the surface of T lymphocytes (T cells) and inhibit the activation of T cells, including CD4<sup>+</sup> T cells, CD8<sup>+</sup> T cells, and regulatory T lymphocytes (Treg cells).<sup>[5]</sup> Ado was also reported to impair the antigen presentation of dendritic cells (DCs), thus inhibiting the downstream immune response.<sup>[5a]</sup> Subsequently, these excess Ado can downregulate immune response of infiltrating immune or inflammatory cells,<sup>[6]</sup> building immune-tolerance

tumor microenvironment.<sup>[7]</sup> Tumor cells utilize Ado-mediated immunosuppressive response to protect tumor tissues against the immune system, thereby evading immune monitoring and promoting tumor progression.<sup>[8]</sup> Regulation of Ado metabolism in the tumor microenvironment is thus applicable for blocking the Ado-mediated immunosuppression and further enhancing the immunotherapeutic efficacy.

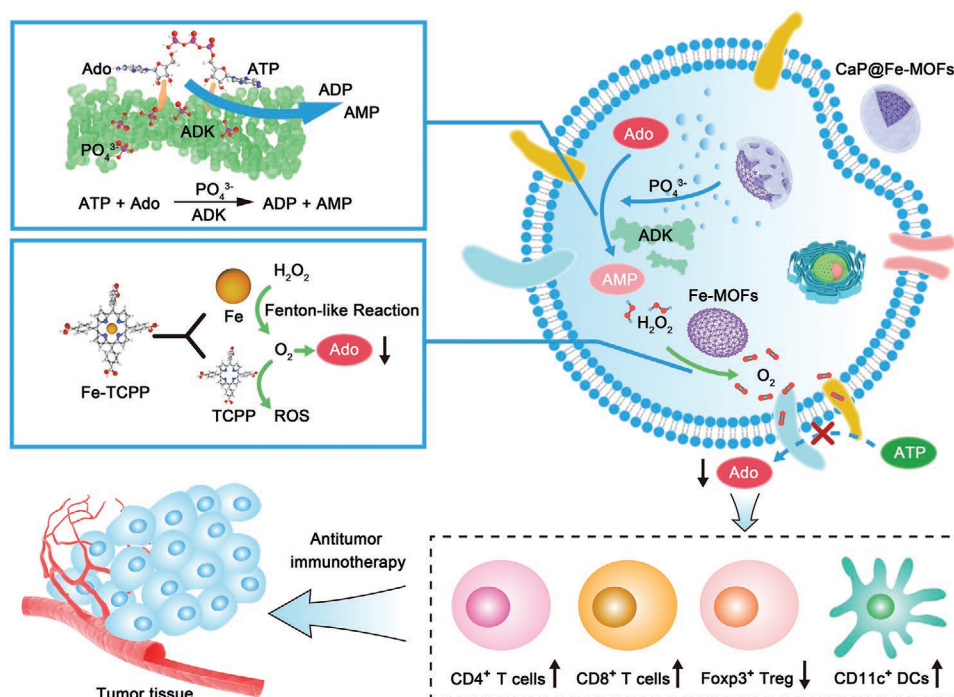
Adenosine kinase (ADK) is the main enzyme that can catalyze the phosphorylation of Ado to adenosine monophosphate (AMP), playing an important role in regulating Ado metabolism.<sup>[9]</sup> Under normal physiological conditions, the catalytic activity of ADK will not be affected by the low level of Ado. In the tumor microenvironment, the active site of ADK can be occupied by a large amount of accumulated Ado, in turn inhibiting the activity of ADK.<sup>[10]</sup> Inorganic phosphate can remove the bound Ado from the active site of ADK via formation of a ternary complex with both ADK and Ado, and subsequently restore the catalytic activity of ADK.<sup>[10,11]</sup> Hence, it would be possible to increase ADK activity by phosphate in the tumor microenvironment, thereby regulating Ado metabolism.

L. Liang, W. Wang, C. Ji, L. Zhang, Y. Jia, Y. Chen, X. Wang, J. Tan, Q. Yuan, W. Tan  
Institute of Chemical Biology and Nanomedicine  
Molecular Science and Biomedicine Laboratory  
State Key Laboratory of Chemo/Biosensing and Chemometrics  
College of Chemistry and Chemical Engineering  
Hunan University  
Changsha 410082, China  
E-mail: tanjie0416@hnu.edu.cn

L.-L. Yang, Z.-J. Sun, Q. Yuan  
The State Key Laboratory Breeding Base of Basic Science of  
Stomatology (Hubei-MOST) and Key Laboratory of Oral Bio-  
medicine Ministry of Education  
School and Hospital of Stomatology  
College of Chemistry and Molecular Sciences  
Wuhan University  
Wuhan 430072, China  
E-mail: sunzj@whu.edu.cn; yuanquan@whu.edu.cn

 The ORCID identification number(s) for the author(s) of this article can be found under <https://doi.org/10.1002/adma.202102271>.

DOI: 10.1002/adma.202102271



**Scheme 1.** Illustration of the designed CaP@Fe-MOFs for blocking Ado-mediated immunosuppressive response via adenosine regulation in the tumor microenvironment. ATP, adenosine triphosphate; Ado, adenosine; ADP, adenosine diphosphate; AMP, adenosine monophosphate; ADK, adenosine kinase; ROS, reactive oxygen species; TCPP, tetrakis (4-carboxyphenyl) porphyrin; Fe-MOFs, iron-based metal-organic frameworks; CaP@Fe-MOFs, calcium phosphate-reinforced iron-based metal-organic frameworks; T cells, T lymphocytes; Treg cells, regulatory T lymphocytes; DCs, dendritic cells.

Inspired by phosphate-induced ADK activity recovery, calcium phosphate-reinforced iron-based metal-organic frameworks (denoted as CaP@Fe-MOFs) were fabricated to reduce Ado in tumor tissues and to inhibit Ado-mediated immunosuppression *in vivo* (Scheme 1). Calcium phosphate coated on CaP@Fe-MOFs was designed to produce inorganic phosphate, restoring the activity of ADK. Subsequently, these phenomena will lead to the reduction of Ado accumulation and the enhancement of antitumor immune response. Fe moieties in CaP@Fe-MOFs can undergo Fenton-like reaction and produce oxygen that can hinder the production of Ado. At the cellular level, the mechanism of Ado downregulation by CaP shell and Fe-MOFs was verified. Moreover, T cells and DCs increased, and Treg cells decreased, indicating that the antitumor immune response was enhanced via Ado regulation by CaP@Fe-MOFs. CaP@Fe-MOFs were finally used for cancer treatment in mice, *in vivo* results show that CaP@Fe-MOFs can alleviate the Ado-mediated immunosuppressive response and exhibit excellent therapeutic effect. These unexpected *in vitro* and *in vivo* findings not only offer a concept for blocking the Ado-mediated immunosuppression but also provide a promising step toward tumor immunotherapy.

## 2. Results and Discussion

The preparation of CaP@Fe-MOFs included the synthesis of Fe-MOFs and the coating of CaP mineralized layer (Figure 1a; Figures S1–S6, Supporting Information). Transmission electron micrograph (TEM) image showed that Fe-MOFs possessed

a well-dispersed nanoshuttle morphology with the homogeneous sizes of about  $70 \pm 10$  nm in length and  $40 \pm 5$  nm in width (Figure 1b; Figure S1, Supporting Information). UV–vis spectroscopy revealed that both tetrakis (4-carboxyphenyl) porphyrin (TCPP) and Fe-MOFs have similar spectra (Figure 1c). Fe-MOFs showed only two absorptions at 500–680 nm, while four peaks were found in the results of TCPP. This observation was ascribed to the increase of molecular symmetry referring to the metalation of TCPP. Moreover, Fourier transform infrared spectroscopy (FT-IR) was utilized to analyze the structure of Fe-MOFs (Figure 1d). Compared to TCPP, the C=O stretch of Fe-MOFs was downshift from 1687 to 1661  $\text{cm}^{-1}$ . An intense Fe–N stretching at 1001  $\text{cm}^{-1}$  and the disappeared N–H bond absorption at 963  $\text{cm}^{-1}$  also reflected the metalation of porphyrin ring with iron.<sup>[12]</sup> Meanwhile, similar to TCPP, Fe-MOFs showed the characteristic peaks for big ring skeleton absorption at 1602, 1550, and 1404  $\text{cm}^{-1}$ , demonstrating that the synthesized Fe-MOFs maintained the pyrrole ring structure of TCPP.<sup>[13]</sup> X-ray photoelectron spectroscopy was performed onto Fe-MOFs for determining the chemical state of Fe species (Figure S2, Supporting Information). The characteristic peak at 398.2 eV in high-resolution N 1s spectrum suggested the formation of Fe–N species. Two relatively weak peaks centered at 711.1 eV (Fe 2p<sub>3/2</sub>) and 724.6 eV (Fe 2p<sub>1/2</sub>) in high-resolution Fe 2p spectrum illustrated partially oxidized Fe species in Fe-MOFs, further providing strong evidence for the existence of Fe–N species.<sup>[14]</sup> TEM image showed that CaP mineralized layer was successfully coated around the Fe-MOFs (Figure 1e). Energy dispersive X-ray (EDX) spectrum also exhibited the characteristic peaks of Ca, P, and Fe with high-intensity signal

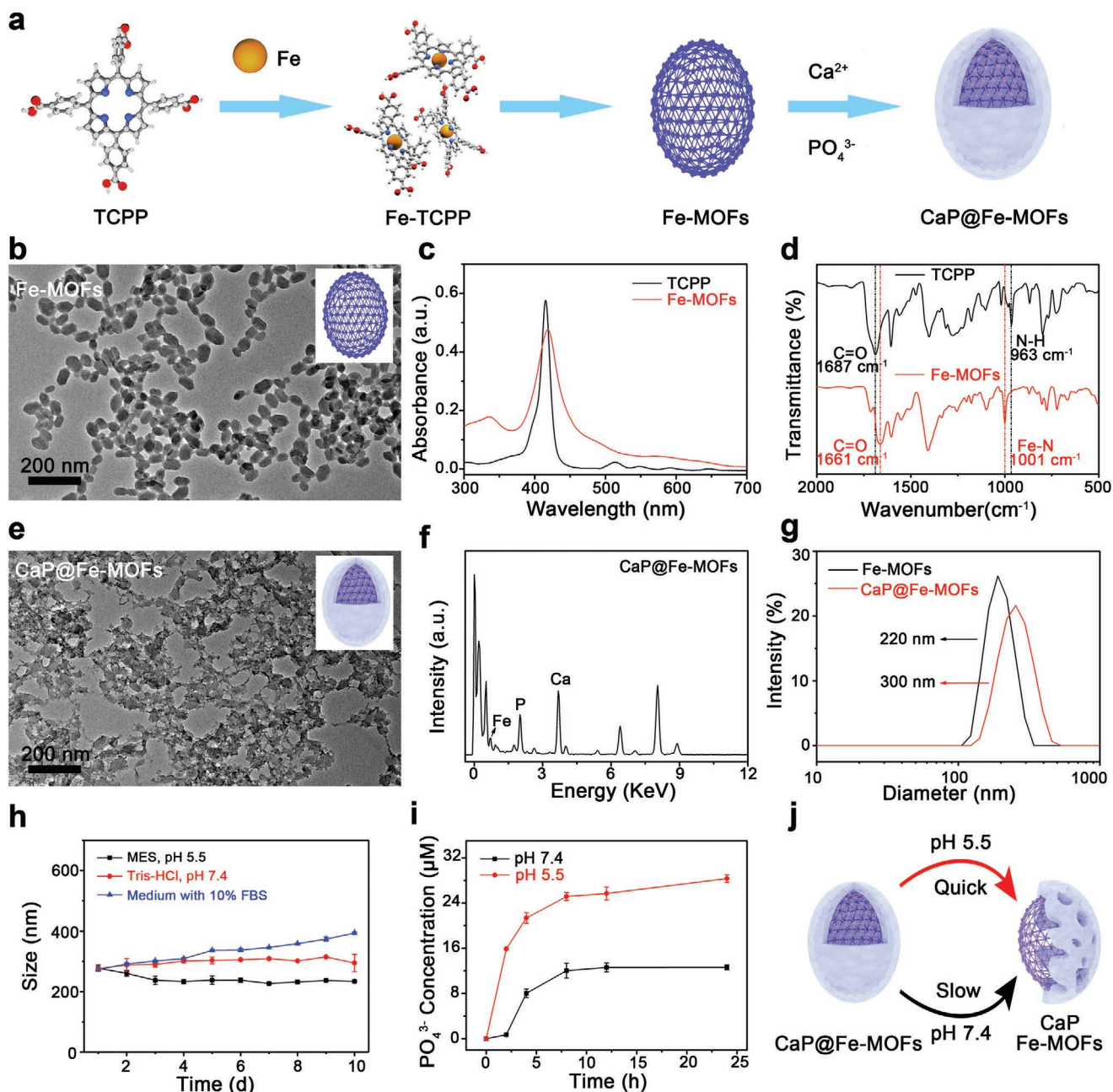


**Figure 1.** Preparation and characterization of CaP@Fe-MOFs. a) Schematic diagram of the preparation of CaP@Fe-MOFs. b) TEM image of Fe-MOFs. c) UV-vis spectra of TCPP and Fe-MOFs. d) FT-IR spectra of TCPP and Fe-MOFs. e) TEM image of CaP@Fe-MOFs. f) EDX of CaP@Fe-MOFs. g) Size determination of Fe-MOFs and CaP@Fe-MOFs via DLS. h) Stability of CaP@Fe-MOFs in different media (MES, black line; Tris-HCl, red line; medium with 10% FBS, blue line). Data are represented as mean  $\pm$  S.D.; ( $n = 3$ ). i) The concentration of phosphate produced by CaP@Fe-MOFs versus time. Data are mean  $\pm$  S.D.; ( $n = 3$ ). j) Schematic diagram of degradation of CaP@Fe-MOFs in acidic solution or in neutral solution.

(Figure 1f), further confirming the successful coating of CaP around the Fe-MOFs. The hydrodynamic diameter of Fe-MOFs and CaP@Fe-MOFs were further determined by dynamic light scattering (DLS). Compared with uncoated Fe-MOFs, CaP@Fe-MOFs showed a slight increase in average size due to the coating of CaP shell (Figure 1g). The stability of CaP@Fe-MOFs was further characterized by DLS in neutral and acidic solution, respectively. In neutral environment, the size of CaP@Fe-MOFs remained unchanged in biological buffers and increased slightly

in serum-containing media that maybe due to the adsorbed protein,<sup>[15]</sup> implying the good stability of CaP@Fe-MOFs (Figure 1h; Figure S4, Supporting Information). While in an acidic solution, CaP@Fe-MOFs showed a weak decrease that may owe to the degradation of CaP shell (Figure 1h). CaP shell can respond to the acidic environment to generate free phosphate ions.<sup>[16]</sup> A phosphate test kit was utilized to detect phosphate<sup>[17]</sup> produced by the degradation of CaP@Fe-MOFs. A fast elevation of phosphate in CaP@Fe-MOFs supernatant

was observed, and phosphate at acidic condition was almost twice as much as that in neutral environment after 24 hours (Figure 1i,j), implying more dissolved CaP@Fe-MOFs and more generated phosphate in acidic solution than that in neutral solution.

According to the reaction 1, with adenosine triphosphate (ATP), ADK could catalyze the phosphorylation of Ado, producing adenosine diphosphate (ADP) and AMP.<sup>[18]</sup>



Due to the high affinity of Ado to ADK and structural similarities of ATP and Ado, Ado can inhibit the activity of ADK by suppressing the binding between ADK and ATP.<sup>[19]</sup> In an acidic environment, the activity of ADK could be regulated by inorganic phosphate in the presence of accumulated Ado.<sup>[10,11]</sup> To investigate whether CaP@Fe-MOFs-produced phosphate can affect ADK-mediated phosphorylation of Ado, ATP, ADP, AMP, and Ado were measured at acidic and normal conditions by high-performance liquid chromatography (HPLC), respectively (Figures S7 and S8, Supporting Information). At acidic condition (pH 5.5) and neutral condition (pH 7.4), compared to the solution without ADK, the solution with ADK showed two new chromatographic peaks with ADP and AMP (Figure S8, Supporting Information). These observations suggested that ADK could catalyze the phosphorylation of Ado, producing ADP and AMP. The chromatographic peaks on the HPLC chromatogram were then quantified. In an acidic environment, with the addition of CaP@Fe-MOFs, the peak intensities of ADP and AMP

increased apparently, indicating the activation of ADK by CaP@Fe-MOFs (Figure 2a; Figure S8a, Supporting Information). In CaP group, similar results could be observed. Comparably, ADP and AMP did not increase with the addition of Fe-MOFs, suggesting that Fe-MOFs cannot promote ADK-mediated phosphorylation. In the neutral environment, for all the groups, the peak intensities of ADP and AMP on the HPLC chromatogram did not increase (Figure 2b; Figure S8b, Supporting Information). By producing a large amount of ADP and AMP as catalytic products, it illustrated that, owing to their CaP shell, CaP@Fe-MOFs could effectively promote ADK-mediated phosphorylation of Ado in acidic solution. Cyclic voltammograms of Ado at different pH were also recorded to evaluate the effect of CaP@Fe-MOFs-produced phosphate on ADK-mediated phosphorylation of Ado (Figure S9, Supporting Information). At acidic condition, the peak current of Ado decreased gradually, showing the decrease of Ado by ADK-mediated phosphorylation (Figure S9a, Supporting Information). Consistent with the chromatographic results, the cyclic voltammetry results also indicated that CaP@Fe-MOFs could promote ADK-mediated phosphorylation of Ado at acidic condition. Altogether, the phosphate produced by CaP@Fe-MOFs can subsequently promote ADK-catalyzed reaction in the acidic environment than that in the neutral environment. As shown in Figure 2c, CaP@Fe-MOFs can decrease the Ado level by promoting the phosphorylation of Ado, generating ADP and AMP in the acidic environment.

Hypoxia in solid tumors has been one of the main drivers for the accumulation of Ado, consequently increasing the tumorigenesis and tumor development.<sup>[20]</sup> In fact, hypoxia and

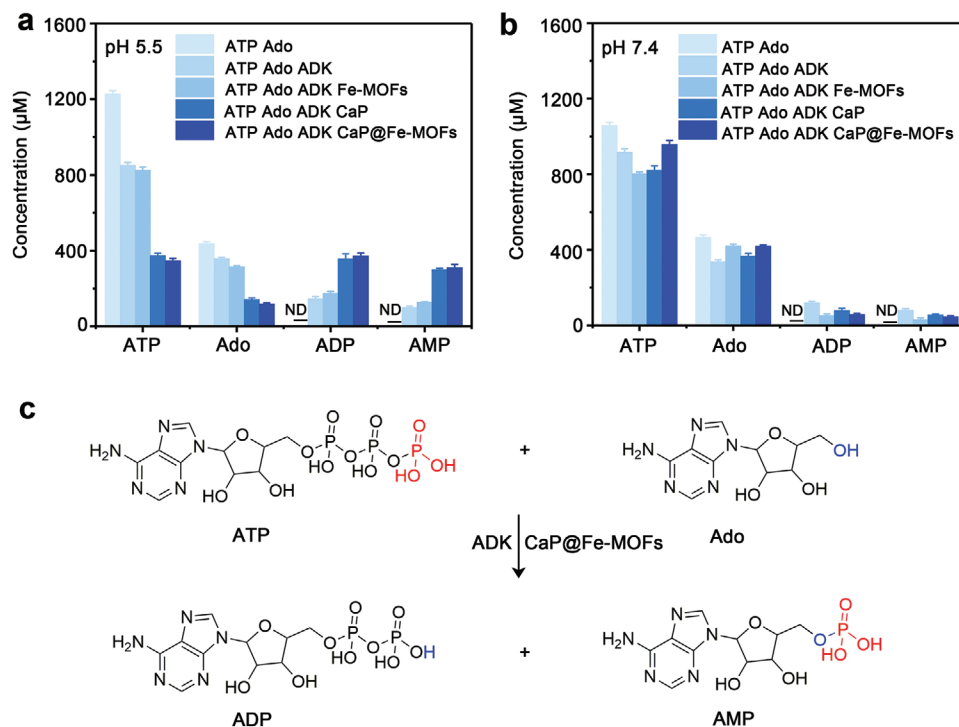


**Figure 2.** Effect of CaP@Fe-MOFs on ADK-mediated phosphorylation of Ado. a) Quantitative analysis of ATP, ADP, AMP, and Ado from HPLC chromatogram in acidic solution with the addition of CaP, Fe-MOFs, or CaP@Fe-MOFs, respectively. b) Quantitative analysis of ATP, ADP, AMP, and Ado from HPLC chromatogram in neutral solution with the addition of CaP, Fe-MOFs, or CaP@Fe-MOFs, respectively. Data are mean  $\pm$  S.D.; ( $n = 3$ ); ND, not detected. c) Schematic showing the involvement of CaP@Fe-MOFs in ADK-mediated phosphorylation of Ado.

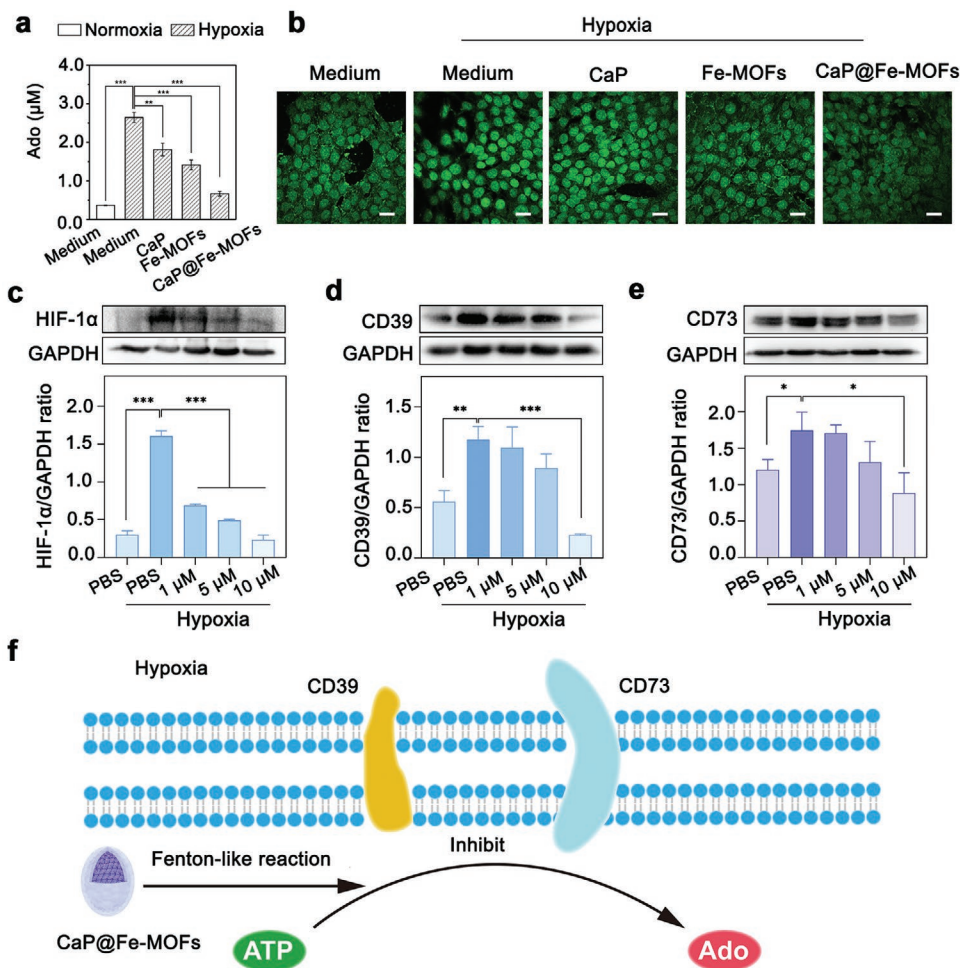


**Figure 3.** In vitro overcoming hypoxia-induced Ado metabolism. a) Ado detection in 4T1 cells under normoxic or hypoxic condition with different treatment. Data are mean  $\pm$  S.D.; ( $n = 3$ ); \* $p < 0.05$ , \*\* $p < 0.01$ , \*\*\* $p < 0.001$  (unpaired two-tailed Student's  $t$ -test). b) Fluorescence images of HIF-1 $\alpha$  in 4T1 cells under normoxic or hypoxic condition after different treatment. Scale bar, 25  $\mu\text{m}$ . c) Western blots of HIF-1 $\alpha$  in 4T1 cells incubated with CaP@Fe-MOFs under normoxic or hypoxic condition. Scale bar, 25  $\mu\text{m}$ . d, e) Western blots and the corresponding quantitative data of CD39 and CD73 in 4T1 cells treated with CaP@Fe-MOFs under normoxic or hypoxic condition. Data are mean  $\pm$  S.D.; ( $n = 3$ ); \* $p < 0.05$ , \*\* $p < 0.01$ , \*\*\* $p < 0.001$  (unpaired two-tailed Student's  $t$ -test). f) Illustration of Ado regulation via Fenton-like reaction of CaP@Fe-MOFs in the hypoxia tumor microenvironment.

its related inducible factor significantly drive the activation of the Ado metabolic changes. Under hypoxic condition, the expression of nucleoside triphosphate diphosphorylase (CD39) and ecto-5-nucleotidase (CD73) increases, promoting the breakdown of ATP into AMP and the hydrolysis of AMP into Ado.<sup>[7c,21]</sup> In the tumor microenvironment, sufficient oxygen supply is the prerequisite for diminishing Ado accumulation by relieving hypoxia and inhibiting the expression of CD39 and CD73.

Fe cluster in frameworks will undergo Fenton-like reaction and produce oxygen that can effectively overcome hypoxia.<sup>[7a,22]</sup> Here, it was investigated whether oxygen produced by Fe moieties in CaP@Fe-MOFs could overcome hypoxia, subsequently inhibiting the hypoxia-driven accumulation of Ado in the tumor microenvironment. To investigate how CaP@Fe-MOFs affects intracellular Ado metabolism under hypoxic condition, mouse breast cancer cells (4T1 cells) were used as the model cells and the hypoxic condition was considered to simulate the tumor microenvironment.<sup>[23]</sup> Western blot results and

fluorescence images proved that hypoxia and CaP@Fe-MOFs treatment would not affect ADK expression (Figures S12 and S13, Supporting Information). Under hypoxic condition, intracellular Ado level was measured by HPLC after the tumor cells were treated with culture medium, CaP, Fe-MOFs, and CaP@Fe-MOFs, respectively (**Figure 3a**; Figure S14, Supporting Information). Under normoxic condition, the peak of Ado was identified and its quantitative value was consistent with the reported Ado level.<sup>[5a,24]</sup> As shown in Figure 3a, in hypoxic environment, the Ado significantly increased and was about six times of that under normoxic condition, demonstrating the accumulation of Ado under hypoxic condition.<sup>[25]</sup> CaP or Fe-MOFs treatment in hypoxic environment induced a decrease of intracellular Ado, while CaP@Fe-MOFs treatment significantly inhibited the intracellular Ado accumulation under hypoxic condition. CaP-caused inhibition of Ado may be contributed to the degradation of CaP that can promote the phosphorylation of Ado. Notably, Fe-MOFs-induced Ado decrease might attribute to the hypoxia alleviation caused by oxygen production. Altogether,

CaP@Fe-MOFs downregulate Ado accumulation in hypoxic environment may not only due to the phosphate generated by CaP, but also owing to the oxygen produced by Fe-MOFs. Oxygen generated by CaP@Fe-MOFs was quantitatively measured by an oxygen sensor. A time-dependent oxygen generation (Figure S15, Supporting Information) indicated that CaP@Fe-MOFs could produce oxygen via Fenton-like reaction. As a downstream marker of hypoxia, the expression of hypoxia inducible factor-1 $\alpha$  (HIF-1 $\alpha$ ) in tumor cells was evaluated by immunofluorescence and western blot to investigate CaP@Fe-MOFs-induced hypoxia suppression.<sup>[26]</sup> As shown in Figure 3b and Figure S16, Supporting Information, both Fe-MOFs-treated group and CaP@Fe-MOFs-treated group displayed weak green fluorescence signal, suggesting the reduced expression of HIF-1 $\alpha$  in tumor cells. Comparably, CaP-treated group showed a strong signal of HIF-1 $\alpha$ , indicating that CaP cannot improve the hypoxia individually. These observations proved that CaP@Fe-MOFs will produce oxygen and achieve hypoxia alleviation via Fenton-like reaction. The effect of different concentration of CaP@Fe-MOFs on the hypoxia alleviation was further measured. As shown in immunofluorescence results, green fluorescence signal from HIF-1 $\alpha$  could be vividly observed in 4T1 cells without CaP@Fe-MOFs treatment and faded in a concentration-dependent manner with CaP@Fe-MOFs (Figures S17 and S18, Supporting Information). In addition, western blot analysis also displayed that the expression of HIF-1 $\alpha$  gradually decreased with the addition of CaP@Fe-MOFs, fitting well with the

immunofluorescence results (Figure 3c). The downregulation of HIF-1 $\alpha$  revealed that CaP@Fe-MOFs can effectively alleviate hypoxia in tumor cells. In particular, hypoxia adjusts the expression of CD39 and CD73 by regulating the activity of HIF-1 $\alpha$ .<sup>[27]</sup> The expression of CD39 and CD73 were evaluated by western blot in CaP@Fe-MOFs incubated tumor cells. As presented in Figure 3d,e, both CD39 and CD73 proteins were gradually downregulated in a dose-dependent manner after treated with CaP@Fe-MOFs under hypoxic condition. The cumulative evidences supported CaP@Fe-MOFs-mediated downregulation of CD39 and CD73 proteins. The intracellular Ado and its metabolites were imaged using a FAM-modified Ado aptamer (Figure S19, Supporting Information). The faded fluorescent signal confirmed that Ado decreased with the addition of CaP@Fe-MOFs. Schematically shown in Figure 3f, in tumor cells under hypoxic condition, CaP@Fe-MOFs-produced oxygen can downregulate the expression of CD39 and CD73, affecting Ado metabolism.

It was important to confirm whether CaP@Fe-MOFs would affect tumor hypoxic environment and hypoxia-induced Ado accumulation in vivo. Tumor tissues from tumor-bearing mice treated with CaP@Fe-MOFs were first stained with anti-HIF-1 $\alpha$  antibody to detect the change of tumor hypoxic environment (Figure 4a). For tumor-bearing mice without CaP@Fe-MOFs treatment, the obviously red fluorescence of HIF-1 $\alpha$  implied the strong tumor hypoxia. After treated with CaP@Fe-MOFs, a significantly decreased red fluorescence of HIF-1 $\alpha$  was observed,

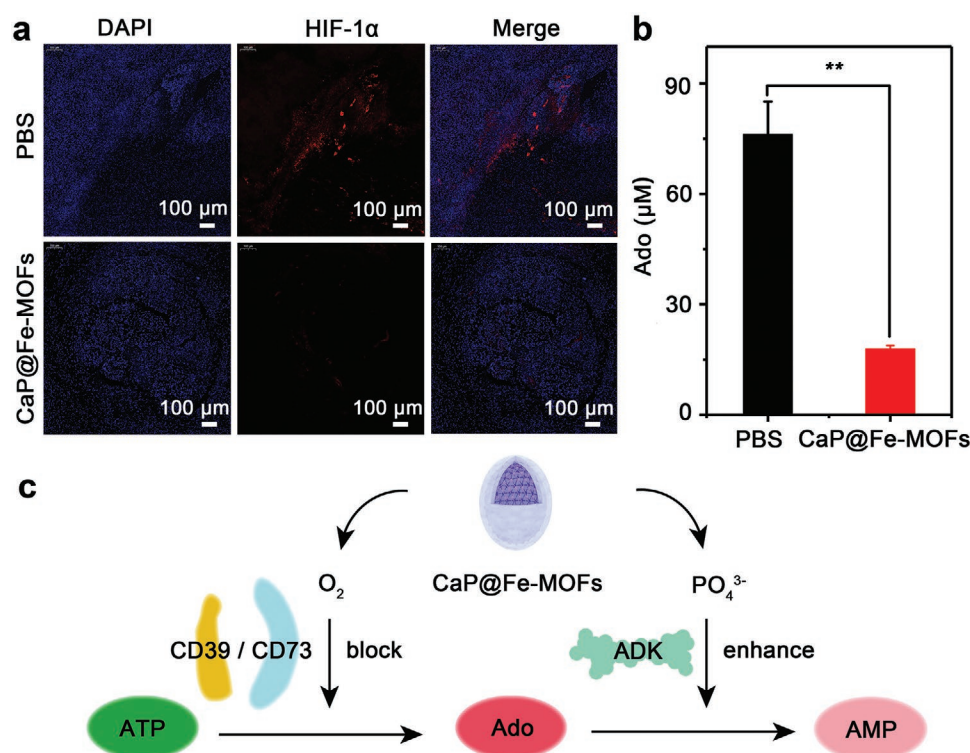


**Figure 4.** In vivo overcoming hypoxia-induced Ado metabolism. a) HIF-1 $\alpha$  immunofluorescence staining of tumor slices from 4T1 tumor-bearing mice treated with CaP@Fe-MOFs. Scale bars: 100  $\mu\text{m}$ . b) Detection of Ado in solid tumor tissues from 4T1 tumor-bearing mice treated with PBS or CaP@Fe-MOFs. Data are mean  $\pm$  S.D.; ( $n = 3$ ); \* $p < 0.05$ ; \*\* $p < 0.01$ ; \*\*\* $p < 0.001$  (unpaired two-tailed Student's  $t$ -test). c) Schematic illustration of Ado metabolism by CaP@Fe-MOFs in the hypoxia tumor microenvironment, including ADK-mediated phosphorylation promoted by phosphate, as well as the generated oxygen via Fenton-like reaction.

demonstrating that CaP@Fe-MOFs greatly weakened tumor hypoxia. The immunofluorescence staining indicated that the overall tumor hypoxia status could be remarkably alleviated after CaP@Fe-MOFs treatment, favorable for Ado decrease. Semiquantitative statistical analysis of hypoxia positive area further indicated that CaP@Fe-MOFs treatment could greatly reduce the tumor hypoxia (Figure S20, Supporting Information). Next, Ado in tumor tissues was detected by HPLC after CaP@Fe-MOFs treatment in the tumor-bearing mice. The peak area of Ado in PBS-treated group was larger than that in CaP@Fe-MOFs-treated group (Figure S21, Supporting Information). Quantitatively, in CaP@Fe-MOFs-treated group, Ado decreased significantly, indicating the CaP@Fe-MOFs-induced inhibition of Ado accumulation (Figure 4b). All the above results demonstrate that CaP@Fe-MOFs will relieve the hypoxic microenvironment and inhibit Ado accumulation in vivo. As shown in Figure 4c, CaP@Fe-MOFs can decrease the Ado, not only attributing to the promoted ADK-mediated phosphorylation, but also to the alleviated hypoxia by oxygen supplement.

A growing number of reports have pointed out that Ado inhibits the activation of immune response,<sup>[4]</sup> playing a notable role in the evasion of antitumor immune response by various immune cells (Figure 5a). As one of the major immune cells, T cells will proliferate and differentiate into a diversity of cells, such as CD4<sup>+</sup> T cells and CD8<sup>+</sup> T cells, that regulate the immune response in cancer immunotherapy.<sup>[28]</sup> It is well established that Ado inhibits T cells activation by signaling primarily through Ado receptors on the surface of T cells.<sup>[5]</sup> Treg cells are a subset of CD4<sup>+</sup> T cells that can use Ado to suppress the function of other T cells.<sup>[29]</sup> Additionally, as an antigen presenting cells, DCs can activate T cells and initiate immune response.<sup>[30]</sup> Ado was reported to impair DC antigen presentation and subsequent T cell activation.<sup>[5a]</sup> Inhibition of Ado is thus able to activate T cells and DCs, relieve the immunosuppressive signal induced by Treg cells, converting an immunosuppressive tumor microenvironment to an immunologically activated environment.<sup>[31]</sup>

Encouraged by the CaP@Fe-MOFs-induced Ado suppression in vitro, the in vivo experiments were carried out to evaluate the anti-tumor efficiency and immune response of CaP@Fe-MOFs. In vivo anti-tumor efficacy and immune response were performed on 4T1 tumor bearing Balb/c mice. Mice were randomly divided into four groups: PBS, CaP, Fe-MOFs, and CaP@Fe-MOFs. Upon tumor suppression assessments, compared with the PBS-treated group, Fe-MOFs and CaP@Fe-MOFs treatment significantly slowed down the tumor growth. Among all the groups, the tumor volume and tumor weight in CaP@Fe-MOFs-treated group were minimum, suggesting the highest antitumor capability of CaP@Fe-MOFs (Figure 5b–d). Histological analysis of tumor sections with hematoxylin and eosin (H&E) staining further showed compact tumor cells in PBS-treated group, and displayed sparse tumor cells in CaP@Fe-MOFs-treated group (Figure 5e). Additionally, body-weight of mice and H&E staining of major organs were also observed (Figures S22 and S23, Supporting Information), demonstrating that CaP@Fe-MOFs have no significant acute toxicity. To assess whether CaP@Fe-MOFs-induced Ado inhibition affects systemic immune response, lymph node from tumor harboring mice was harvested. As immunity-associated cells, CD4<sup>+</sup>

T cells, CD8<sup>+</sup> T cells, Foxp3<sup>+</sup> Treg cells, and CD11c<sup>+</sup> DCs were subsequently analyzed using flow cytometry. Compared with the PBS-treated mice, the population of CD4<sup>+</sup> T cells and CD8<sup>+</sup> T cells increased in the tumor draining lymph node of CaP@Fe-MOFs-injected mice (Figure 5f,g). The populations of Foxp3<sup>+</sup> Treg in CD4<sup>+</sup> T cells were significantly decreased after CaP@Fe-MOFs treatment (Figure 5h,i), suggesting that CaP@Fe-MOFs relieved Foxp3<sup>+</sup> Treg cells-mediated immunosuppression. Additionally, CD11c<sup>+</sup> DCs cells also increased significantly as the immunologically activated cells (Figure 5j,k; Figure S24, Supporting Information). In CaP-treated group, a small percentage of CD4<sup>+</sup>, CD8<sup>+</sup> T cells, and DCs cells were observed. By contrast, high percentage of CD4<sup>+</sup>, CD8<sup>+</sup> T cells, and DCs cells were found in the Fe-MOFs-treated group, suggesting that immunosuppression was alleviated and immune response was activated by Fe-MOFs treatments.<sup>[32]</sup> Consequently, after CaP@Fe-MOFs treatment, CD4<sup>+</sup> T cells, CD8<sup>+</sup> T cells, and CD11c<sup>+</sup> DCs increased, Foxp3<sup>+</sup> Treg cells decreased, indicating that the antitumor immune response was enhanced via Ado regulation by CaP@Fe-MOFs. For all the groups, the in vivo immune activation extent was approximately consistent with their Ado inhibition ability at the cellular level. Immunofluorescence staining of tumor slices was also performed to further investigate CD4, CD8, Foxp3, and CD11c expression in tissues. CaP@Fe-MOFs-treated group showed widely distributed red fluorescence signal from CD4 and green fluorescence signal from CD8, implying the high infiltration level of CD4<sup>+</sup> T cells and CD8<sup>+</sup> T cells in CaP@Fe-MOFs-treated group (Figure 5l,m). Semiquantitative results of CD4, CD8 positive area further indicated that CaP@Fe-MOFs treatment could greatly increase the expression of CD4 and CD8, consisting with the flow cytometry results (Figure S25a,b, Supporting Information). For immunofluorescence staining of Foxp3 (Figure 5n), the vivid red fluorescence of Foxp3 implied the high infiltration level of Foxp3<sup>+</sup> Treg cells in PBS treated group. In CaP@Fe-MOFs-treated group, a significantly decreased red fluorescence was observed, demonstrating the downregulation of Foxp3<sup>+</sup> Treg cells. Statistically, immunofluorescence staining of Foxp3 indicated that Foxp3<sup>+</sup> Treg cells were strongly suppressed in the tumor microenvironment after CaP@Fe-MOFs injection (Figure S25c, Supporting Information), fitting well with the previous flow cytometry results. Immunofluorescence staining of CD11c visually indicated the marked increase of CD11c<sup>+</sup> DCs cells in the tumor microenvironment after CaP@Fe-MOFs treatment (Figure 5o; Figure S25d, Supporting Information). All these CaP@Fe-MOFs-induced immune responses verified that CaP@Fe-MOFs treatment effectively reduced Ado immunosuppression and eventually significantly improved treatment efficiency. Collectively, with the regulation of Ado metabolism, CaP@Fe-MOFs not only enhance the antitumor immune response in vivo, but also exhibit excellent tumor inhibition effect.

### 3. Conclusion

In summary, CaP@Fe-MOFs were designed to reduce Ado accumulation in the tumor microenvironment and to inhibit Ado-mediated immunosuppressive response. In an acidic solution and at the cellular condition, CaP@Fe-MOFs could regulate the

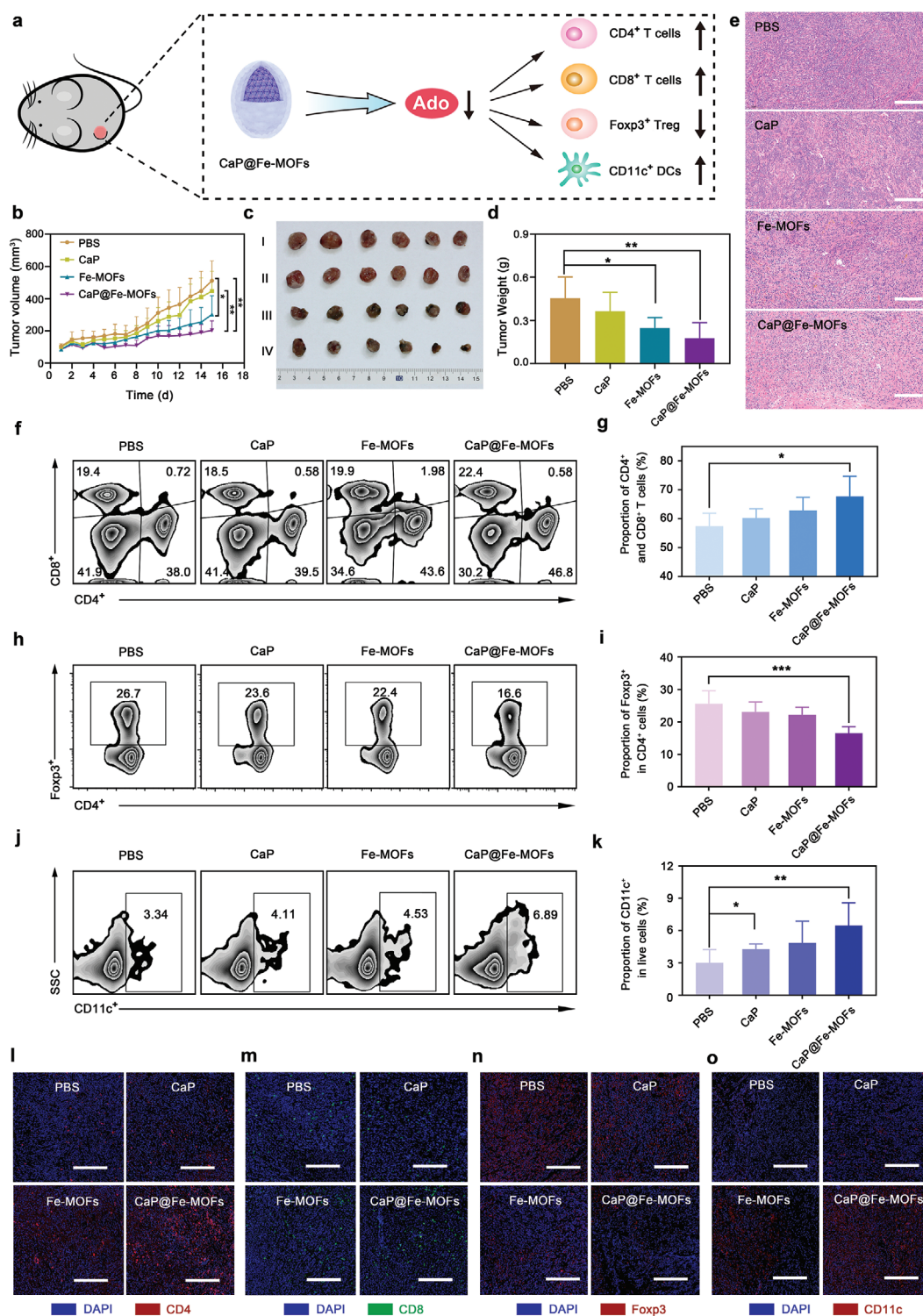


**Figure 5.** In vivo anticancer effect and immune response of CaP@Fe-MOFs. a) Schematic illustration of using CaP@Fe-MOFs to block Ado-mediated immunosuppressive response in 4T1 tumor-bearing mice. b) Tumor growth curve after different treatments. c) Photograph of resected tumors after different treatments. I, PBS; II, CaP; III, Fe-MOFs; IV, CaP@Fe-MOFs. d) Final weight of tumor tissue after different treatments. e) Representative H&E staining of tumor sections after different treatments; Scale bars, 200  $\mu$ m. f,g) Representative flow cytometric analysis images and relative quantification of CD4<sup>+</sup> and CD8<sup>+</sup> T cells. h,i) Representative flow cytometric analysis images and relative quantification of Foxp3<sup>+</sup> Treg cells. j,k) Representative flow cytometric analysis images and relative quantification of CD11c<sup>+</sup> DCs cells. Data are presented as mean  $\pm$  S.D.; ( $n = 6$ ); \* $p < 0.05$ ; \*\* $p < 0.01$ ; \*\*\* $p < 0.001$  (unpaired two-tailed Student's  $t$ -test). l) Representative immunofluorescence images from tumor showing CD4<sup>+</sup> T cells; Scale bars, 200  $\mu$ m. m) Representative immunofluorescence images from tumor showing CD8<sup>+</sup> T cells; Scale bars, 200  $\mu$ m. n) Representative immunofluorescence images showing Foxp3<sup>+</sup> Treg cells; Scale bars, 200  $\mu$ m. o) Representative immunofluorescence images showing CD11c<sup>+</sup> cells; Scale bars, 200  $\mu$ m.



Ado metabolism by promoting ADK-catalyzed Ado phosphorylation and relieving the hypoxic tumor microenvironment. Additionally, CaP@Fe-MOFs were used for blocking the Ado-mediated immunosuppression and enhancing the cancer treatment in mice. In vivo results of immune response showed that T cells and DCs significantly increased while Treg cells decreased by CaP@Fe-MOFs-induced Ado decrease. Taken together, CaP@Fe-MOFs could not only enhance the antitumor immune response by reducing Ado, but also exhibit excellent tumor inhibition effect. For cancer immunotherapy, many nanomedicines have been tested in clinical trials.<sup>[33]</sup> However, immunotherapy nanomedicines show antitumor effect only in subsets of patients, since tumors can deploy multiple mechanisms to avoid immunosurveillance.<sup>[34]</sup> As one of many normal immune regulatory factors or immune checkpoints, Ado can be hijacked by tumors to avoid immune attack.<sup>[35]</sup> Blocking the inhibitory effect of Ado on the immune response, Ado-regulating nanomedicines are expected to assist with other checkpoint inhibitors and promote immunotherapy. This finding provides insights into Ado metabolism and reveals a new direction for Ado-mediated immunosuppression research.

## Supporting Information

Supporting Information is available from the Wiley Online Library or from the author.

## Acknowledgements

L.L., L.-L.Y., and W.W. contributed equally to this work. This work was supported by the National Key R&D Program of China (2017YFA0208000), National Natural Science Foundation of China (21925401, 21904037, 81874131), and Natural Science Foundation of Hunan Province (No. 2020JJ5038). The animal experimental protocol was approved by the Experimental Animal Ethics Committee of the School and Hospital of Stomatology at Wuhan University (2018LUNSHENZIA28).

## Conflict of Interest

The authors declare no conflict of interest.

## Data Availability Statement

Research data are not shared.

## Keywords

adenosine, adenosine kinase, immunosuppression, metal-organic frameworks

Received: March 23, 2021

Revised: July 26, 2021

Published online:

[1] a) J.-F. Chen, H. K. Eltzschig, B. B. Fredholm, *Nat. Rev. Drug Discovery* **2013**, *12*, 265; b) K. A. Jacobson, M. L. Reitman, *Cells* **2020**, *9*, 956.

- [2] a) J. Blay, T. D. White, D. W. Hoskin, *Cancer Res.* **1997**, *57*, 2602; b) J. Szychala, *Pharmacol. Ther.* **2000**, *87*, 161.
- [3] a) K. Synnestvedt, G. T. Furuta, K. M. Comerford, N. Louis, J. Karhausen, H. K. Eltzschig, K. R. Hansen, L. F. Thompson, S. P. Colgan, *J. Clin. Invest.* **2002**, *110*, 993; b) J. C. Morote-Garcia, P. Rosenberger, J. Kuhlicke, H. K. Eltzschig, *Blood* **2008**, *111*, 5571.
- [4] a) D. Mittal, A. Young, K. Stannard, M. Yong, M. W. Teng, B. Allard, J. Stagg, M. J. Smyth, *Cancer Res.* **2014**, *74*, 3652; b) M. V. Sitkovsky, D. Lukashov, S. Apasov, H. Kojima, M. Koshiba, C. Caldwell, A. Ohta, M. Thiel, *Annu. Rev. Immunol.* **2004**, *22*, 657; c) T. Gnad, S. Scheibler, I. von Kugelgen, C. Scheele, A. Kilic, A. Glode, L. S. Hoffmann, L. Reverte-Salisa, P. Horn, S. Mutlu, A. El-Tayeb, M. Kranz, W. Deuther-Conrad, P. Brust, M. E. Lidell, M. J. Betz, S. Enerback, J. Schrader, G. G. Yegutkin, C. E. Muller, A. Pfeifer, *Nature* **2014**, *516*, 395.
- [5] a) D. Vijayan, A. Young, M. W. L. Teng, M. J. Smyth, *Nat. Rev. Cancer* **2017**, *17*, 765; b) S. Deaglio, K. M. Dwyer, W. Gao, D. Friedman, A. Usheva, A. Erat, J.-F. Chen, K. Enjyoji, J. Linden, M. Oukka, V. K. Kuchroo, T. B. Strom, S. C. Robson, *J. Exp. Med.* **2007**, *204*, 1257.
- [6] L. Antonioli, C. Blandizzi, P. Pacher, G. Hasko, *Nat. Rev. Cancer* **2013**, *13*, 842.
- [7] a) J. Stagg, M. J. Smyth, *Oncogene* **2010**, *29*, 5346; b) A. Ohta, M. Sitkovsky, *Front. Immunol.* **2014**, *5*, 304; c) B. Allard, P. A. Beavis, P. K. Darcy, J. Stagg, *Curr. Opin. Pharmacol.* **2016**, *29*, 7.
- [8] A. Ohta, *Front. Immunol.* **2016**, *7*, 109.
- [9] a) U. K. Decking, G. Schlieper, K. Kroll, J. Schrader, *Circ. Res.* **1997**, *81*, 154; b) D. Boison, *Pharmacol. Rev.* **2013**, *65*, 906; c) Y. Yamada, H. Goto, N. Ogasawara, *Biochim. Biophys. Acta* **1981**, *660*, 36.
- [10] M. Maj, B. Singh, R. S. Gupta, *Biochim. Biophys. Acta* **2000**, *1476*, 33.
- [11] J. Park, B. Singh, M. C. Maj, R. S. Gupta, *Protein J.* **2004**, *23*, 167.
- [12] a) L. Cui, J. Wu, J. Li, H. Ju, *Anal. Chem.* **2015**, *87*, 10635; b) T. Sato, W. Mori, C. N. Kato, E. Yanaoka, T. Kuribayashi, R. Ohtera, Y. Shiraishi, *J. Catal.* **2005**, *232*, 186.
- [13] P. Ling, J. Lei, H. Ju, *Biosens. Bioelectron.* **2015**, *71*, 373.
- [14] L. Jiao, G. Wan, R. Zhang, H. Zhou, S. H. Yu, H. L. Jiang, *Angew. Chem., Int. Ed.* **2018**, *57*, 8525.
- [15] a) M. Lundqvist, J. Stigler, G. Elia, I. Lynch, T. Cedervall, K. A. Dawson, *Proc. Natl. Acad. Sci. U. S. A.* **2008**, *105*, 14265; b) M. P. Monopoli, D. Walczyk, A. Campbell, G. Elia, I. Lynch, F. Baldelli Bombelli, K. A. Dawson, *J. Am. Chem. Soc.* **2011**, *133*, 2525; c) C. Wang, B. Chen, M. He, B. Hu, *ACS Nano* **2021**, *15*, 3108.
- [16] a) J. Kim, H. R. Cho, H. Jeon, D. Kim, C. Song, N. Lee, S. H. Choi, T. Hyeon, *J. Am. Chem. Soc.* **2017**, *139*, 10992; b) H. P. Rim, K. H. Min, H. J. Lee, S. Y. Jeong, S. C. Lee, *Angew. Chem., Int. Ed.* **2011**, *50*, 8853.
- [17] a) X. Wan, H. Zhong, W. Pan, Y. Li, Y. Chen, N. Li, B. Tang, *Angew. Chem., Int. Ed.* **2019**, *58*, 14134; b) Y. Wang, X. Hu, L. Zhang, C. Zhu, J. Wang, Y. Li, Y. Wang, C. Wang, Y. Zhang, Q. Yuan, *Nat. Commun.* **2019**, *10*, 2829.
- [18] D. Köhler, A. Streienberger, J. C. Morote-García, T. F. Granja, M. Schneider, A. Straub, D. Boison, P. Rosenberger, *Crit. Care Med.* **2016**, *44*, e181.
- [19] a) M. Mimouni, F. Bontemps, G. Van den Berghe, *Biochem. Pharmacol.* **1995**, *50*, 1587; b) MathewsII, M. D. Erion, S. E. Ealick, *Biochemistry* **1998**, *37*, 15607.
- [20] M. V. Sitkovsky, S. Hatfield, R. Abbott, B. Belikoff, D. Lukashov, A. Ohta, *Cancer Immunol. Res.* **2014**, *2*, 598.
- [21] A. M. Chambers, S. Matosevic, *Front. Mol. Biosci.* **2019**, *6*, 60.
- [22] a) G. Lan, K. Ni, Z. Xu, S. S. Veroneau, Y. Song, W. Lin, *J. Am. Chem. Soc.* **2018**, *140*, 5670; b) J. Mo, Y. Xu, L. Zhu, W. Wei, J. Zhao, *Angew. Chem., Int. Ed.* **2021**, *60*, 12524; c) J. Chen, H. Gao, Z. Li, Y. Li, Q. Yuan, *Chin. Chem. Lett.* **2020**, *31*, 1398.
- [23] a) J. Liu, Y. Liu, W. Bu, J. Bu, Y. Sun, J. Du, J. Shi, *J. Am. Chem. Soc.* **2014**, *136*, 9701; b) R. Xu, Y. Wang, X. Duan, K. Lu, D. Micheroni, A. Hu, W. Lin, *J. Am. Chem. Soc.* **2016**, *138*, 2158.

- [24] M. de Lera Ruiz, Y. H. Lim, J. Zheng, *J. Med. Chem.* **2014**, *57*, 3623.
- [25] S. Serra, S. Deaglio, *J. Visualized Exp.* **2016**, *113*, 54124.
- [26] Q. F. Li, X. R. Wang, Y. W. Yang, H. Lin, *Cell Res.* **2006**, *16*, 548.
- [27] G. L. Semenza, *Trends Pharmacol. Sci.* **2012**, *33*, 207.
- [28] A. Lanzavecchia, F. Sallusto, *Science* **2000**, *290*, 92.
- [29] a) G. Borsellino, M. Kleinewietfeld, D. Di Mitri, A. Sternjak, A. Diamantini, R. Giometto, S. Hopner, D. Centonze, G. Bernardi, M. L. Dell'Acqua, P. M. Rossini, L. Battistini, O. Rotzschke, K. Falk, *Blood* **2007**, *110*, 1225; b) F. Y. Mao, H. Kong, Y. L. Zhao, L. S. Peng, W. Chen, J. Y. Zhang, P. Cheng, T. T. Wang, Y. P. Lv, Y. S. Teng, X. L. Fu, Y. G. Liu, X. L. Wu, C. J. Hao, N. You, P. Luo, P. W. Yu, Q. M. Zou, G. Guo, Y. Zhuang, *Cell Death Dis.* **2017**, *8*, e3002; c) L. Mao, T. F. Fan, L. Wu, G. T. Yu, W. W. Deng, L. Chen, L. L. Bu, S. R. Ma, B. Liu, Y. Bian, A. B. Kulkarni, W. F. Zhang, Z. J. Sun, *J. Cell. Mol. Med.* **2017**, *21*, 2199.
- [30] E. Panther, S. Corinti, M. Idzko, Y. Herouy, M. Napp, A. la Sala, G. Girolomoni, J. Norgauer, *Blood* **2003**, *101*, 3985.
- [31] P. Rosenberger, J. M. Schwab, V. Mirakaj, E. Masekowsky, A. Mager, J. C. Morote-Garcia, K. Unertl, H. K. Eltzschig, *Nat. Immunol.* **2009**, *10*, 195.
- [32] a) S. Zanganeh, G. Hutter, R. Spitler, O. Lenkov, M. Mahmoudi, A. Shaw, J. S. Pajarinen, H. Nejadnik, S. Goodman, M. Moseley, L. M. Coussens, H. E. Daldrup-Link, *Nat. Nanotechnol.* **2016**, *11*, 986; b) E. Ploetz, A. Zimpel, V. Cauda, D. Bauer, D. C. Lamb, C. Haisch, S. Zahler, A. M. Vollmar, S. Wuttke, H. Engelke, *Adv. Mater.* **2020**, *32*, 1907267.
- [33] Y. Shi, *Adv. Ther.* **2020**, *3*, 1900215.
- [34] a) K. Shao, S. Singha, X. Clemente-Casares, S. Tsai, Y. Yang, P. Santamaria, *ACS Nano* **2015**, *9*, 16; b) P. Zhang, Y. Zhai, Y. Cai, Y. Zhao, Y. Li, *Adv. Mater.* **2019**, *31*, 1904156.
- [35] K. Garber, *Nat. Biotechnol.* **2017**, *35*, 805.